How to cite: *Angew. Chem. Int. Ed.* **2025**, e202423403
doi.org/10.1002/anie.202423403

Radical Biocatalysis

Biocatalytic Olefin Difunctionalization for Synthesis of Chiral 2-Azidoamines Using Nonheme Iron Enzymes

Anthony J. Huls[+], *Jordi Soler*[+], *Yuxuan Su, Yunfang Yang, Marc Garcia-Borràs,* and Xiongyi Huang**

Abstract: Alkene difunctionalization represents an important category of reactions in organic synthesis, with a diverse array of transformations developed over the past decades for various synthetic applications. Nevertheless, the scope and diversity of biocatalytic alkene difunctionalization have been limited, constraining its synthetic utility. In this study, we repurposed nonheme iron enzymes to generate iron nitrene intermediates for alkene difunctionalization. 4-hydroxymandelate synthase from *Amycolatopsis orientalis* (*Ao*HMS) was successfully engineered for direct alkene aminoazidation to produce chiral 2-azidoamines. Directed evolution was performed on *Ao*HMS to provide evolved variants that could utilize *O*-pivaloylhydroxylamine triflic acid as the nitrene precursor and produced various primary aminoazidation products with up to 44% yield, 44 total turnover number (TTN), and 98.5:1.5 enantiomeric ratio (e.r.). Mechanistic studies indicated that this new biocatalytic transformation proceeds through a stepwise radical addition and azide recombination pathway. This work expands the catalytic toolbox of metalloenzymes and opens up new opportunities for biosynthesis by introducing nonnatural olefin difunctionalization reactions into biocatalysis.

Alkene difunctionalization represents an important class of transformations in contemporary organic synthesis. These reactions involve the addition of two functionalities to carbon–carbon double bonds, offering a direct and adaptable approach to creating molecular complexity using readily available alkene starting materials. Over the past decades, there has been significant development of synthetic methods across various domains of chemical catalysis to facilitate these transformations.[1–9] These advances not only impact chemical synthesis from the laboratory to industrial scale but also give rise to new concepts for molecular functionalization and push the frontiers of organic synthesis.

In sharp contrast to the rapid progress and large diversity of alkene difunctionalization methods in synthetic chemistry, there are far fewer biological approaches to achieve this reaction.[10] Most biological approaches for olefin difunctionalization rely on a multienzymatic strategy, wherein alkenes are initially transformed into intermediate products, such as epoxides, and subsequently elaborated with additional enzymatic steps to yield difunctionalized products (Figure 1a).[10,11] There are few biocatalytic transformations that can directly convert alkenes to their difunctionalized products, such as alkene dihydroxylation catalyzed by Rieske dioxygenases,[12] halohydroxylation catalyzed by vanadium-dependent haloperoxidases (VHPOs),[13] and halocyclization catalyzed by VHPOs and flavin-dependent halogenases (FDHs) (Figure 1a).[13,14] Recently, the development of enzymes for nonnatural transformations has introduced novel biocatalytic pathways for olefin difunctionalization. These innovations include alkene carboazidation catalyzed by a dirhodium-containing streptavidin-based artificial metalloenzyme,[15] alkene amino hydroxylation catalyzed by heme proteins,[16] alkene trifluoromethyl azidation catalyzed by nonheme iron enzymes,[17,18] photocatalytic alkene carbo-oxygenation catalyzed by ene-reductases,[19,20] atom transfer radical cyclization catalyzed by engineered cytochrome P450s,[21] and photocatalytic alkene difunctionalization to afford enantioenriched ketones via thiamine-dependent enzymes.[22] Despite this progress, in comparison to synthetic alkene difunctionalization reactions, biocatalysis still lags in terms of reaction diversity, with many synthetically important olefin difunctionalization reactions inaccessible to biocatalysis.

We envision that nonheme iron enzymes hold immense potential for establishing versatile catalytic platforms for alkene difunctionalization. Among all metalloproteins, nonheme iron enzymes are particularly well-suited for incorporating new synthetic reaction pathways into biocatalysis for two main reasons: First, they exhibit broad structural and

[*] Dr. A. J. Huls[+], Y. Su, Prof. Dr. X. Huang
Department of Chemistry, Johns Hopkins University, 3400 North Charles Street, Baltimore, MD 21218, USA
E-mail: xiongyi@jhu.edu

Dr. J. Soler[+], Dr. M. Garcia-Borràs
Institut de Química Computacional i Catàlisi, and Departament de Química, Universitat de Girona, C/ M. Aurèlia Capmany, 69, Girona 17003, Spain
E-mail: marc.garcia@udg.edu

Prof. Dr. Y. Yang
College of Chemical Engineering, Zhejiang University of Technology, Hangzhou, Zhejiang 310014, China

[+] Both authors contributed equally to this work.

Additional supporting information can be found online in the Supporting Information section

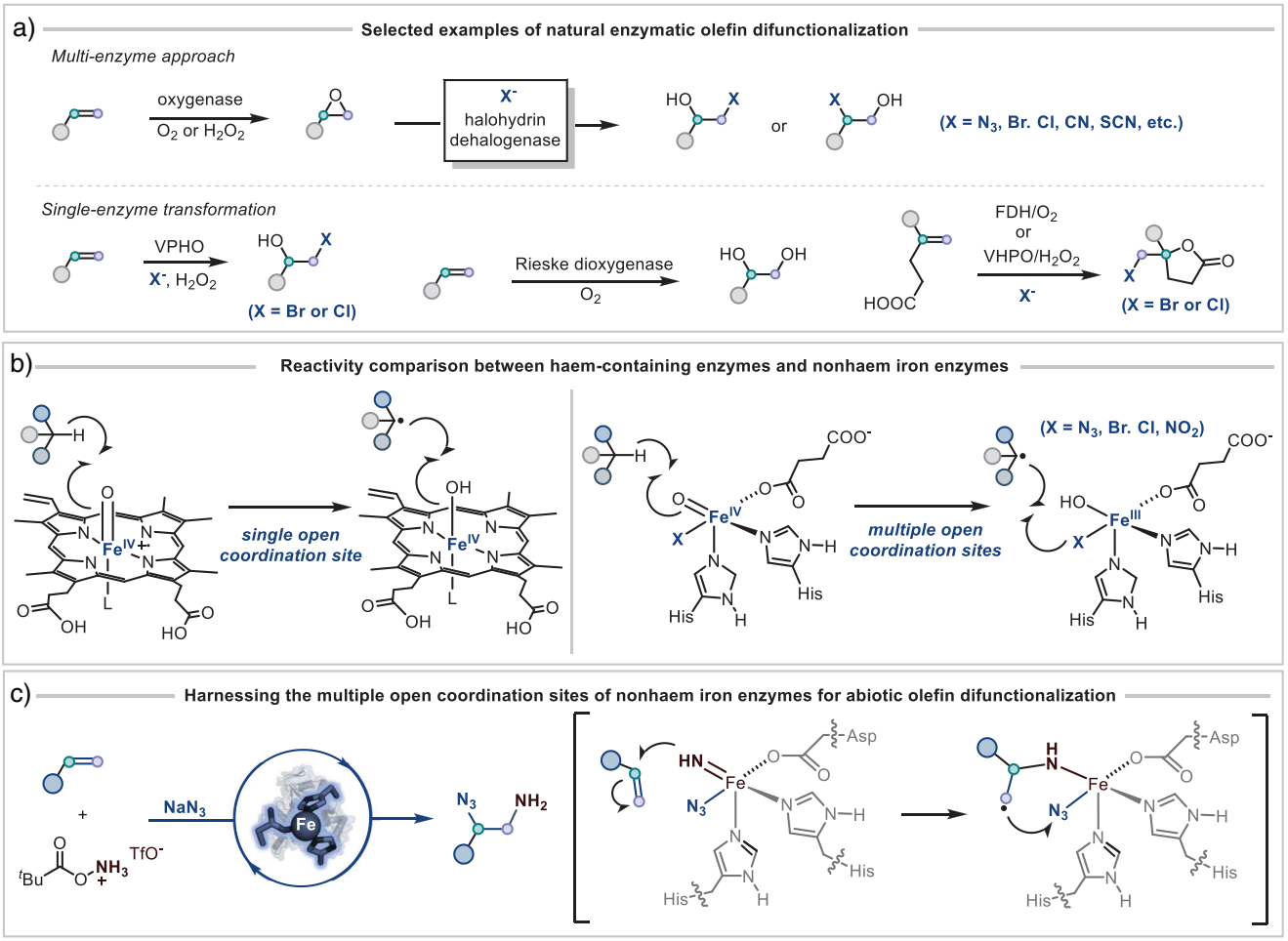

Figure 1. Conceptualization of nonnatural olefin difunctionalization catalyzed by nonheme iron enzymes. a) Representative examples of natural multienzymatic strategies[19,20] and single-enzyme strategies[22–25,27] for olefin difunctionalization. VHPO stands for vanadium-dependent haloperoxidase. FDH stands for flavin-dependent halogenase. b) Comparison of natural activities of heme-dependent enzymes and nonheme iron enzymes. The multiple open coordination sites of nonheme iron enzymes allows for more reaction modes other than C–H hydroxylation such as C–H halogenation and azidation. c) Leveraging nonheme iron enzymes for new-to-nature olefin difunctionalization reactions.

functional diversity with greater operational simplicity compared to many other metalloenzymes involved in molecular functionalization.[23,24] Secondly, in contrast to heme-protein-based biocatalysts, nonheme iron enzymes possess diverse metal binding configurations and high coordination flexibility of the metal center.[25–27] These attributes enable nonheme iron enzymes catalyze reactions that are inherently inaccessible to single-site heme-protein catalysts, such as redirecting the oxygen rebound mechanism of iron-oxo complexes for carbon–heteroatom bond formation (Figure 1b).[28,29] These features also enable the incorporation of a broad range of nonnative reaction modes into biocatalysis, including radical-relay C–H functionalization,[30–32] Lewis acid catalysis,[33–36] metallophotoredox decarboxylative functionalization,[37,38] metal-hydride-mediated reduction and hydration,[39,40] iron–nitrene catalysis,[41–44] and redox activation of iodine(III) reagents for radical transformations.[17,18]

In this study, we aim to harness the remarkable tunability of nonheme iron enzymes to introduce new alkene difunctionalization reactions into biocatalysis. Specifically, our objective is to reprogram natural nonheme iron enzymes to generate iron–nitrene intermediates for alkene aminoazidation (Figure 1c). This transformation holds significant importance in organic synthesis as it offers an efficient way to access a diverse range of molecules featuring vicinal diamino functionalities, which are crucial structural motifs in numerous bioactive compounds.[45,46] Our design for this reaction draws inspiration from three recent developments in both chemocatalysis and biocatalysis. First, prior works in synthetic catalysis have illustrated that iron-based synthetic catalysts can produce nitrene intermediates for alkene difunctionalization through a stepwise radical addition and recombination pathway.[47–50] Secondly, nonheme iron enzymes have recently been shown to form iron–nitrene intermediates within their active sites.[41–44] These studies, coupled with the established capacity of nonheme iron enzymes for radical group transfer reactions,[17,30–32,37,38,51–53] provide support for the feasibility of this new-to-nature enzymatic transformation. If successfully developed, this reaction would not only expand the scope of biocatalytic nitrene transfer reactions but also offer a

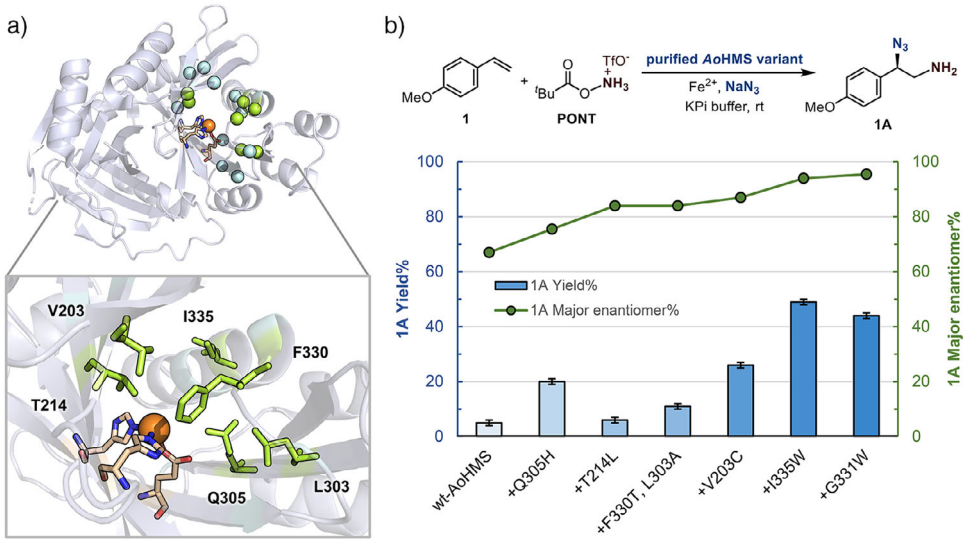

Figure 2. Optimization of *Ao*HMS via directed evolution. a) Active site residues selected for site-saturation mutagenesis (SSM) and screening. The figure was generated using PyMOL based on the crystal structure of wild-type *Ao*HMS (PDB: 2R5V). Residues with beneficial mutations identified are depicted as green spheres in the upper figure and further illustrated as green sticks in the lower figure. Residues subjected to SSM but without identified beneficial mutations are represented as cyan spheres in the upper figure. For further details, refer to Table S3. b) Representative variants identified during the directed evolution of *Ao*HMS. Experimental details see Table S4. The determination of the product absolute configuration is detailed in the section VII of the Supporting Information.

genetically tunable and sustainable alternative to chemical methods for alkene difunctionalization.

With this mechanistic analysis in hand, we initiated our investigation by evaluating a range of nonheme iron enzymes for their performance in a model aminoazidation reaction with *p*-methoxystyrene as the substrate and *O*-pivaloylhydroxylamine triflic acid (PONT) as the nitrene precursor (Figure 2 and Table S1). Our initial screening was conducted using cell lysates, and enzymes displaying promising initial activity were subsequently subjected to further assessment in purified protein form. Through these experiments, we found that the 4-hydroxymandelate synthase from *Amycolatopsis orientalis* (*Ao*HMS) could yield the desired aminoazidation product with 1.8% yield and 62:38 enantiomeric ratio (e.r.). To validate this initial activity, we conducted a series of control experiments (Table S2). Removing the enzyme catalyst from the reaction decreased the product yield to 0.5%. Furthermore, mutating the two iron-binding histidines to alanines reduced the yield to 0.7% and the enantioselectivity to 48:52 e.r. These findings collectively indicate that the observed enantioselective transformation is mediated by the iron center in the active site of *Ao*HMS.

We next aimed to enhance the catalytic performance of *Ao*HMS in this nonnatural transformation through directed evolution (Figure 2). HMS naturally catalyzes the C–H hydroxylation of 4-hydroxyphenylpyruvate (HPP) to produce 4-hydroxymandalate (HMA) during the biosynthesis of non-proteinogenic macrocyclic peptide antibiotics.[54] The native substrate, HPP, binds to the iron center of HMS via bidentate coordination. This binding arrangement is stabilized by an intricate hydrogen-bonding network involving residues Q305, S201, T214, G331, and an active-site water molecule (see the mechanistic section for detailed discussion). Additionally, a hydrophobic pocket formed by residues F330, Y339, I335, F188, and I216 accommodates the phenol moiety of HPP.[55] We hypothesized that these active site components that promote the native reaction of *Ao*HMS would need to be reconfigured to enhance the aminoazidation. In this regard, we conducted sequential site-saturation mutagenesis (SSM) and screening on these nine residues as well as additional residues located nearby (Table S3). The first beneficial mutation identified was Q305H, which increased the yield from 5% to 20% and improved the enantioselectivity from 67:33 e.r. to 75.5:24.5 e.r. Incorporation of the T214L mutation further enhanced the e.r. to 84:16, albeit with a decrease in yield to 6%. In subsequent rounds, the addition of F330T and L303A doubled the yield to 11%, and the V203C mutation led to another twofold increase, reaching a yield of 26%. During this stage, enantioselectivity improved only marginally, from 84:16 to 87:13 e.r. A major improvement was achieved with the I335W mutation, which enhanced both the yield (to 49%) and the enantioselectivity (to 94:6 e.r.). Finally, introducing the G331W mutation yielded the final variant *Ao*HMS T214L/V203C/L303A/Q305H/F330T/G331W/I335W (referred to as $AoHMS_{AmAz}$), which delivered the model aminoazidation product in 44% yield, 44 total turnover number (TTN) and 95.5:4.5 e.r. (Figure 2b and Tables S3–S5). Notably, the reaction proceeded very rapidly, with the time-course data showing that product formation reached saturation within the first minute (Table S6).

With $AoHMS_{AmAz}$ in hand, we proceeded to explore the substrate scope of this enzymatic transformation (Figure 3a). The reaction exhibited versatility with respect to a range of aromatic substitution patterns of styrene, and it tolerated common functional groups such as halogens, nitro, and

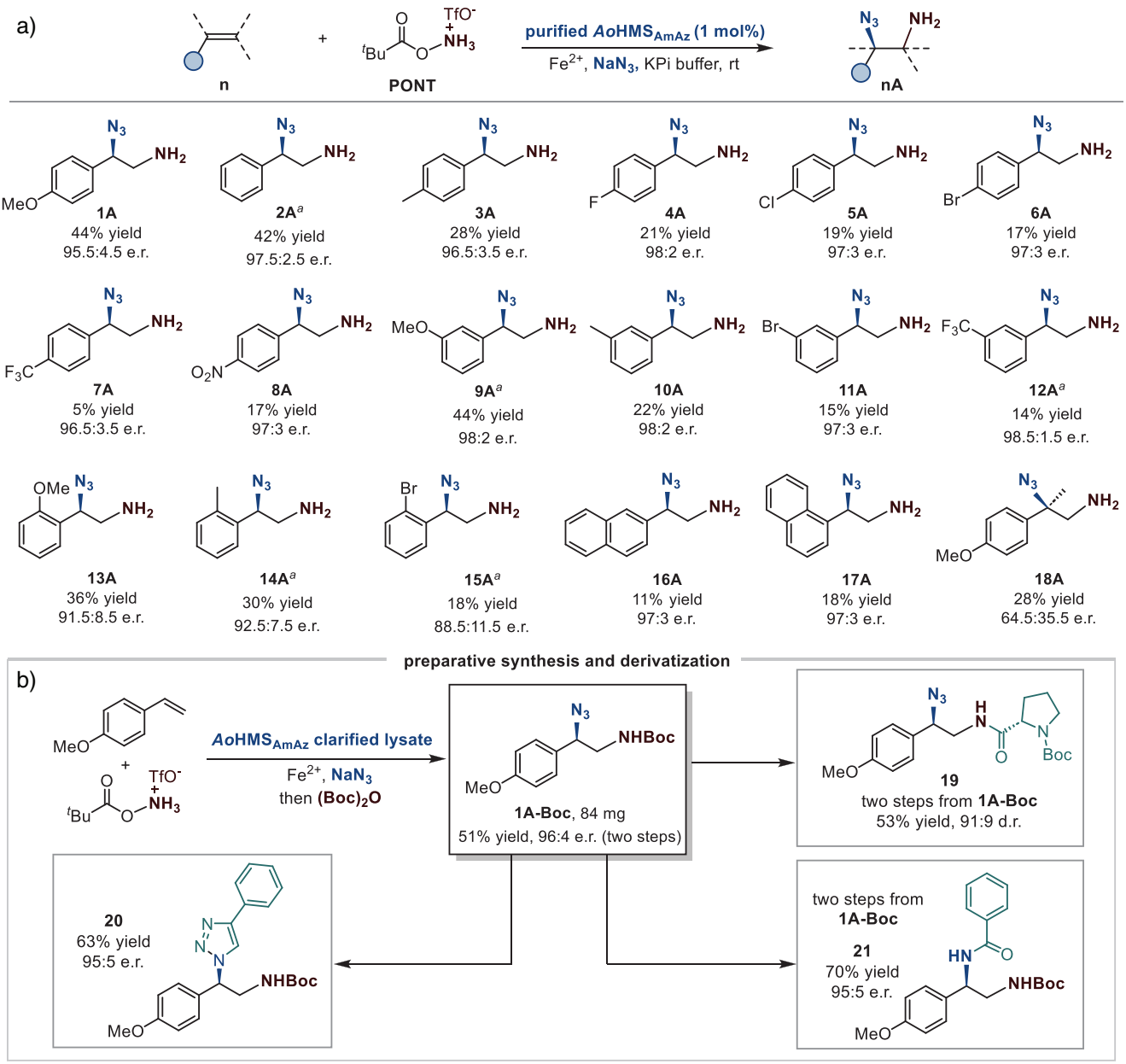

Figure 3. Substrate scope and preparative synthesis. a) Substrate scope test. Experiments were performed with purified *Ao*HMS$_{AmAz}$ with procedures detailed in section (H) of the Supporting Information. The concentrations of each reaction component are 50 μM enzyme, 125 μM Fe^{2+}, 5 mM substrate, 50 mM NaN_3, 10 mM ascorbic acid, and 5 mM PONT. Reactions were carried out at room temperature for 1.5 h. [a]Reaction was performed with 100 μM enzyme (2 mol% catalyst loading). b) Preparative synthesis. Detailed conditions see section VIII of the Supporting Information.

methoxy groups. High enantioselectivity was achieved for substrates bearing diverse *para*- and *meta*-substituents, with all enantioselectivities exceeding 95:5 e.r. Substrates with *ortho*-substituents displayed slightly lower enantioselectivity, ranging from 88.5:11.5 e.r. to 92.5:7.5 e.r. The method was also suitable for 1,1-disubstituted alkene substrates, albeit with reduced enantioselectivity. These results indicate that the reaction is sensitive to the steric environment surrounding the alkene reaction center. It is also worth noting that unactivated olefins and α,β-unsaturated esters are not active substrates in this biocatalytic transformation (Figure S1). We next evaluated the utility of our reaction for preparative-scale synthesis. To achieve this, we further optimized the reaction in cell lysate (Tables S7) to bypass the laborious steps of protein purification and enhanced the operational simplicity of this transformation. With the optimized protocol, we successfully obtained a Boc-protected aminoazidation product on a 75 mg scale with 96:4 e.r. and 51% yield over two steps (Figure 3b). Leveraging both the azide and amine groups as reaction handles, we converted this product into various difunctionalized chiral compounds using well-established methods, including copper-catalyzed azide–alkyne cycloaddition and azide reduction (section VIII of the Supporting Information and Figure 3b). This demonstration

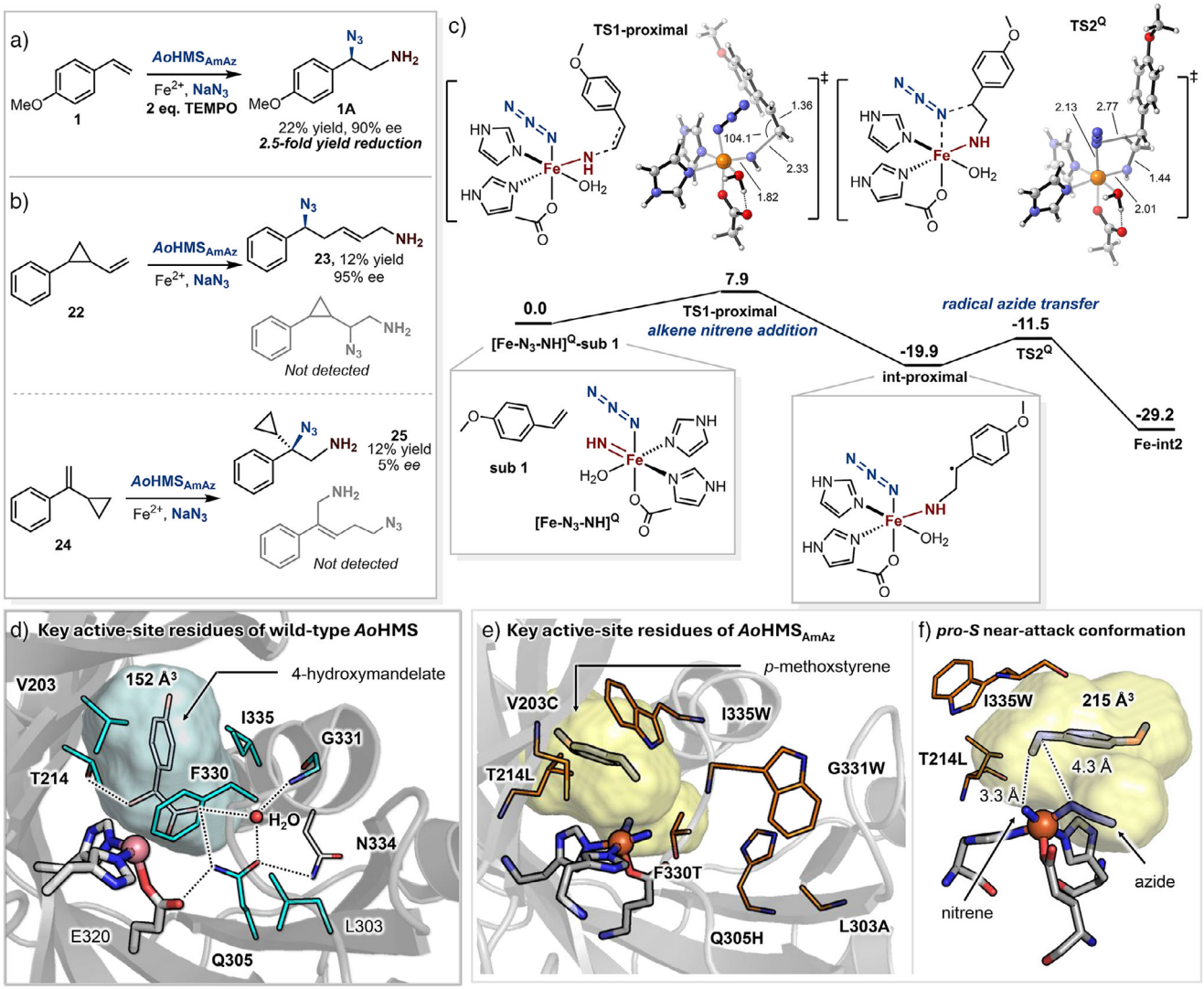

Figure 4. Mechanistic studies. a) TEMPO trapping experiment. b) Radical clock studies. c) Reaction energy barriers obtained from DFT calculations employing a truncated active-site model. d) Key active-site residues of wild-type *Ao*HMS and cavity analysis. The analysis was performed with the crystal structure of wild-type *Ao*HMS (PDB: 2R5V). e) Active-site analysis of *Ao*HMS$_{AmAz}$ with *p*-methoxystyrene bound, based on a representative snapshot from MD simulations. f) Most favorable binding mode of p-methoxystyrene in the active site of *Ao*HMS$_{AmAz}$ characterized from MD simulations, which corresponds to a *pro-S* near-attack conformation. (energies in kcal mol-1, distances in Å, and angles in degrees, see section XI of the Supporting Information for details of computational studies).

underscored the potential of our biocatalytic platform to generate molecular complexity from simple starting materials.

We conducted a series of experiments to gain a deeper understanding of the mechanistic aspects of this enzymatic reaction. The addition of TEMPO to the reaction led to a two-fold decrease in the reaction yield. This observation aligns with prior reports on aminoazidation reactions catalyzed by iron triflate and suggests a radical mechanism (Figure 4a).[50] To further investigate the radical nature of the transformation, we utilized two radical clock substrates with differing rates of ring-opening rearrangement (Figure 4b). Our findings revealed that the radical clock with a slow ring-opening rate exclusively produced the unrearranged product, while the ultrafast radical clock solely generated the ring-opening product. These results provide additional evidence for a stepwise mechanism and rule out the formation of an aziridine intermediate. However, we could not discount the involvement of a cationic intermediate formed via a further oxidation of the carbon-centered radical generated after the initial nitrene addition to the alkene substrate.

We subsequently conducted density functional theory (DFT) calculations to investigate the mechanism of this reaction (Figure 4c). We used a truncated model where iron was coordinated with two imidazoles and an acetate to examine the intrinsic reaction barriers within a 2-histidine-1-carboxylate iron coordination environment, excluding effects from other protein residues. This model revealed that the lowest-energy spin state for the iron–nitrene intermediate is a quintet, aligning with prior experimental and computational studies of iron–nitrene intermediates.[56–59] We next explored the radical addition of nitrene to alkene substrate **1** using the quintet iron–nitrene complex. Our findings revealed that

the alkene can approach the iron–nitrene intermediate in two major conformations (Figure S2), which primarily differ in the relative position of the alkene to the iron-bound azide. In the proximal conformation (**TS1-proximal**, Figures 4c and S2), the alkene addition positions the generated carbon-centered radical close to the iron-bound azide, facilitating azide transfer. In contrast, the distal conformation places the alkene further from the iron-bound azide (**TS1-distal**, Figure S2), causing the generated carbon-centered radical to recombine with the nitrene nitrogen, yielding the aziridination product. Intriguingly, the distal conformation has a lower intrinsic barrier for alkene nitrene addition (3.9 kcal mol^{-1}, **TS1-distal**, Figure S2) compared to the proximal addition (7.9 kcal mol^{-1}, **TS1-proximal**, Figures 4c and S2). These results suggest the critical role of the enzyme active site in properly orienting the substrate and the covalently linked radical intermediate to favor the azide transfer pathway (Figure 4c and S2) over the lower-energy radical cyclization pathway (Figure S2). We next studied the radical azide transfer step and obtained an energy barrier of 8.4 kcal mol^{-1}. Due to steric constraints imposed by the covalent linkage between the substrate radical and the iron center, the radical recombines with the iron-bound nitrogen of the azide rather than the terminal nitrogen, contrasting with the radical-relay C–H azidation previously reported by our group.[37] Additionally, we analyzed the energy profile for this reaction using a protonated iron–nitrene intermediate and obtained similar energy barriers for all steps (Figure S3). While determining the protonation state of the iron–nitrene intermediate when formed in the enzymatic framework remains challenging, our calculations support a comparable stepwise radical reaction mechanism in both scenarios.

To further investigate how the introduced mutations impact the reaction, we performed molecular dynamics (MD) simulations. Figure 4d highlights key active-site residues of wild-type *Ao*HMS based on its crystal structure. V203, T214, I335, and F330 form the substrate-binding pocket. T214 also forms a hydrogen bond with the hydroxyl group of the product, 4-hydroxymandelate, suggesting its potential role in facilitating the native hydroxylation reaction. Q305 is involved in a hydrogen-bonding network that includes the iron-coordinating residue E320, the substrate HPP/product 4-hydroxymandelate, N334 in the C-terminal α-helix, and a key active-site water molecule. This water plays a critical role in the native HMS reaction by forming multiple hydrogen bonds, particularly with G331, a conserved residue among HMS homologs that regulates the dynamics of the C-terminal α-helix and influences HMS catalysis.[55,60] In contrast, these native active-site features are largely disrupted in the evolved variant *Ao*HMS_{AmAz} for aminoazidation (Figures 4e and Figure S4S). The mutations V203C, T214L, I335W, and F330T reshape the binding pocket into a new hydrophobic cavity, accompanied by notable conformational changes in the loop region connecting to the C-terminal α-helix. Additionally, the Q305H and L303A mutations disrupt the original hydrogen-bonding network involving the active-site water, with Q305H now oriented outward from the active site. The G331W mutation at the hinge region further alters the active-site environment. Together, these changes generate an enlarged active-site pocket (~215 $Å^3$), which accommodates the styrene substrate in a conformation favorable for interaction with the iron–nitrene intermediate in a *pro-S* near-attack conformation, leading to the formation of the (*S*)-enantiomer of the product (Figure 4f).

In summary, we have established a versatile biocatalytic platform utilizing nonheme iron enzymes for alkene difunctionalization through iron–nitrene reaction pathway. The successful adaptation of nonheme iron enzymes for this transformation highlights the versatility and broad applicability of this biocatalytic platform. We anticipate that this study will catalyze further advancements in enzymatic methods for olefin difunctionalization and expand the scope of metalloenzymatic catalysis to encompass valuable synthetic transformations previously unknown in biocatalysis.

Acknowledgements

The authors thank Dr. Phil Mortimer and the JHU Mass Spectrometry Facility for analytical support. Financial support was provided by the Johns Hopkins University and the National Institute for General Medical Sciences R35GM147639 (to X. H.). This work was also supported by the Spanish MICINN (Ministerio de Ciencia e Innovación) PID2022-141676NB-I00 and TED2021-130173B-C42 projects (to M.G.B), and the Ramón y Cajal program via the RYC 2020–028628-I fellowship (to M.G.B), the Generalitat de Catalunya (2021SGR00623 project to M.G.B.), and the Spanish MIU (Ministerio de Universidades) predoctoral fellowship FPU18/02380 (to J.S.), and the Ramon Areces Foundation for a postdoctoral Fellowship (to J.S.). This work was also supported by the National Natural Science Foundation of China (22371256, 21978272) (to Y.Y.), the Fundamental Research Funds for the Provincial Universities of Zhejiang (RF-C2022006) (to Y.Y.).

Conflict of Interests

The authors declare no conflict of interest.

Data Availability Statement

All data required to assess the conclusions of this study are included in the main paper, the supplementary materials, or can be obtained from the authors upon reasonable request.

Keywords: Nitrenes · Nonheme iron enzymes · Olefin difunctionalization · Radical biocatalysis

[1] H. Yao, W. Hu, W. Zhang, *Molecules* **2021**, *26*, 105.
[2] J. Lin, R.-J. Song, M. Hu, J.-H. Li, *Chem. Rec.* **2019**, *19*, 440–451.
[3] Z.-L. Li, G.-C. Fang, Q.-S. Gu, X.-Y. Liu, *Chem. Soc. Rev.* **2020**, *49*, 32–48.
[4] R. I. McDonald, G. Liu, S. S. Stahl, *Chem. Rev.* **2011**, *111*, 2981–3019.

[5] J. Derosa, O. Apolinar, T. Kang, V. T. Tran, K. M. Engle, *Chem. Sci.* **2020**, *11*, 4287–4296.
[6] R. K. Dhungana, K. C. Shekhar, P. Basnet, R. Giri, *Chem. Rec.* **2018**, *18*, 1314–1340.
[7] M.-Y. Cao, X. Ren, Z. Lu, *Tetrahedron Lett.* **2015**, *56*, 3732–3742.
[8] S. O. Badir, G. A. Molander, *Chem* **2020**, *6*, 1327–1339.
[9] G. S. Sauer, S. Lin, *ACS Catal.* **2018**, *8*, 5175–5187.
[10] S. Wu, Y. Zhou, Z. Li, *Chem. Commun.* **2019**, *55*, 883–896.
[11] M. Huff, D. Telford, *Trends Pharmacol. Sci.* **2005**, *26*, 335–340.
[12] S. M. Barry, G. L. Challis, *ACS Catal.* **2013**, *3*, 2362–2370.
[13] G. T. Höfler, A. But, F. Hollmann, *Org. Biomol. Chem.* **2019**, *17*, 9267–9274.
[14] D. Mondal, B. F. Fisher, Y. Jiang, J. C. Lewis, *Nat. Commun.* **2021**, *12*, 3268.
[15] T. K. Hyster, L. Knörr, T. R. Ward, T. Rovis, *Science* **2012**, *338*, 500–503.
[16] I. Cho, C. K. Prier, Z. J. Jia, R. K. Zhang, T. Görbe, F. H. Arnold, *Angew. Chem. Int. Ed.* **2019**, *58*, 3138–3142.
[17] J. G. Zhang, A. J. Huls, P. M. Palacios, Y. Guo, X. Huang, *J. Am. Chem. Soc.* **2024**, *146*, 34878–34886.
[18] H. He, J.-X. Yan, J.-X. Zhu, S.-J. Liu, X.-Q. Liu, P. Chen, X. Wang, Z.-J. Jia, *Angew. Chem. Int. Ed.* **2025**, *64*, e202423507.
[19] Y. Ouyang, J. Turek-Herman, T. Qiao, T. K. Hyster, *J. Am. Chem. Soc.* **2023**, *145*, 17018–17022.
[20] J. Yu, Q. Zhang, B. Zhao, T. Wang, Y. Zheng, B. Wang, Y. Zhang, X. Huang, *Angew. Chem. Int. Ed.* **2024**, *63*, e202402673.
[21] Q. Zhou, M. Chin, Y. Fu, P. Liu, Y. Yang, *Science* **2021**, *374*, 1612–1616.
[22] Z. Xing, F. Liu, J. Feng, L. Yu, Z. Wu, B. Zhao, B. Chen, H. Ping, Y. Xu, A. Liu, Y. Zhao, C. Wang, B. Wang, X. Huang, *Nature* **2025**, *637*, 1118–1123.
[23] C. Q. Herr, R. P. Hausinger, *Trends Biochem. Sci* **2018**, *43*, 517–532.
[24] E. I. Solomon, D. E. DeWeese, J. T. Babicz, *Biochemistry* **2021**, *60*, 3497–3506.
[25] E. L. Hegg, L. Que, *Eur. J. Biochem.* **1997**, *250*, 625–629.
[26] C. A. Joseph, M. J. Maroney, *Chem. Commun.* **2007**, 3338.
[27] L. C. Blasiak, F. H. Vaillancourt, C. T. Walsh, C. L. Drennan, *Nature* **2006**, *440*, 368–371.
[28] A. Papadopoulou, F. Meyer, R. M. Buller, *Biochemistry* **2023**, *62*, 229–240.
[29] J. M. Bollinger Jr., W.-C. Chang, M. L. Matthews, R. J. Martinie, A. K. Boal, C. Krebs, in *2-Oxoglutarate-Dependent Oxygenases* (Ed: C. Schofield and R. Hausinger), The Royal Society of Chemistry, Cambridge, UK **2015**, pp. 95–122.
[30] J. Rui, Q. Zhao, A. J. Huls, J. Soler, J. C. Paris, Z. Chen, V. Reshetnikov, Y. Yang, Y. Guo, M. Garcia-Borràs, X. Huang, *Science* **2022**, *376*, 869–874.
[31] Q. Zhao, Z. Chen, J. Soler, X. Chen, J. Rui, N. T. Ji, Q. E. Yu, Y. Yang, M. Garcia-Borràs, X. Huang, *Nat. Synth.* **2024**, *3*, 958–966.
[32] L.-P. Zhao, B. K. Mai, L. Cheng, F. Gao, Y. Zhao, R. Guo, H. Wu, Y. Zhang, P. Liu, Y. Yang, *Nat. Synth.* **2024**, *3*, 967–975.
[33] W. Ghattas, V. Dubosclard, S. Tachon, M. Beaumet, R. Guillot, M. Réglier, A. J. Simaan, J.-P. Mahy, *Angew. Chem. Int. Ed.* **2019**, *58*, 14605–14609.
[34] N. Fujieda, H. Ichihashi, M. Yuasa, Y. Nishikawa, G. Kurisu, S. Itoh, *Angew. Chem. Int. Ed.* **2020**, *59*, 7717–7720.
[35] J. Zhang, Q. Zhang, R. Ge, A. Liu, B. Chen, Z. Zhang, B. Zhao, J. Yu, Y. Zhao, L. Yu, M. Cao, B. Wang, X. Huang, *Angew. Chem. Int. Ed.* **2025**, *64*, e202500338.
[36] X. Mu, X. Ji, X. Chen, H. Wu, J. Rui, X. Hong, M. M. Worth, A. D. Reitz, L. T. M. Goldberg, M. Garcia-Borràs, S. L. J. Michel, Y. Yang, X. Huang, *Nat. Catal.* **2025**, *8*, 635–644.
[37] J. Rui, X. Mu, J. Soler, J. C. Paris, Y. Guo, M. Garcia-Borràs, X. Huang, *Nat. Catal.* **2024**, *7*, 1394–1403.
[38] L.-P. Zhao, K. Lin, P.-P. Xie, H. Liu, H. Xiang, X. Liu, Y. Zhao, P. Liu, Y. Yang, *Angew. Chem. Int. Ed.* **2025**, *64*, e202506361.
[39] B. Wang, Y. Lu, L. Cha, T.-Y. Chen, P. M. Palacios, L. Li, Y. Guo, W.-c. Chang, C. Chen, *Angew. Chem. Int. Ed.* **2023**, *62*, e202311099.
[40] Z. Wan, X. Zhang, H. Zhuang, Z. Xie, L. Yu, Z. Fu, Y. Sun, W. Wang, R. Wu, P. Ji, *Nat. Synth.* **2025**, 1–11. https://doi.org/10.1038/s44160-025-00788-6.
[41] N. W. Goldberg, A. M. Knight, R. K. Zhang, F. H. Arnold, *J. Am. Chem. Soc.* **2019**, *141*, 19585–19588.
[42] M. A. Vila, V. Steck, S. R. Giordano, I. Carrera, R. Fasan, *ChemBioChem* **2020**, *21*, 1981–1987.
[43] M. Davidson, M. McNamee, R. Fan, Y. Guo, W.-c. Chang, *J. Am. Chem. Soc.* **2019**, *141*, 3419–3423.
[44] L.-P. Zhao, H. Liu, B. K. Mai, Y. Zhang, L. Cheng, P. Liu, Y. Yang, *Nat. Chem. Biol.* **2025**, 1–10. https://doi.org/10.1038/s41589-025-01953-w.
[45] S. De Jong, D. G. Nosal, D. J. Wardrop, *Tetrahedron* **2012**, *68*, 4067–4105.
[46] S. R. S. Saibabu Kotti, C. Timmons, G. Li, *Chem. Biol. Drug Des.* **2006**, *67*, 101–114.
[47] D.-F. Lu, C.-L. Zhu, J. D. Sears, H. Xu, *J. Am. Chem. Soc.* **2016**, *138*, 11360–11367.
[48] L. Legnani, B. Morandi, *Angew. Chem. Int. Ed.* **2016**, *55*, 2248–2251.
[49] L. Legnani, G. Prina-Cerai, T. Delcaillau, S. Willems, B. Morandi, *Science* **2018**, *362*, 434–439.
[50] S. Makai, E. Falk, B. Morandi, *J. Am. Chem. Soc.* **2020**, *142*, 21548–21555.
[51] M. L. Matthews, W.-C. Chang, A. P. Layne, L. A. Miles, C. Krebs, J. M. Bollinger, *Nat. Chem. Biol.* **2014**, *10*, 209–215.
[52] C. A. Gomez, D. Mondal, Q. Du, N. Chan, J. C. Lewis, *Angew. Chem. Int. Ed.* **2023**, *62*, e202301370.
[53] V. Yadav, L. Wen, S. Yadav, M. A. Siegler, D. P. Goldberg, *Inorg. Chem.* **2023**, *62*, 17830–17842.
[54] B. K. Hubbard, M. G. Thomas, C. T. Walsh, *Chem. Biol.* **2000**, *7*, 931–942.
[55] J. Brownlee, P. He, G. R. Moran, D. H. T. Harrison, *Biochemistry* **2008**, *47*, 2002–2013.
[56] S. Chatterjee, I. Harden, G. Bistoni, R. G. Castillo, S. Chabbra, M. van Gastel, A. Schnegg, E. Bill, J. A. Birrell, B. Morandi, F. Neese, S. DeBeer, *J. Am. Chem. Soc.* **2022**, *144*, 2637–2656.
[57] A. Radović, N. J. Wolford, H. Li, W. W. Brennessel, H. Xu, M. L. Neidig, *Organometallics* **2023**, *42*, 1810–1817.
[58] D. A. Iovan, T. A. Betley, *J. Am. Chem. Soc.* **2016**, *138*, 1983–1993.
[59] Y. Zhou, J. Ni, Z. Lyu, Y. Li, T. Wang, G.-J. Cheng, *ACS Catal.* **2023**, *13*, 1863–1874.
[60] P. He, G. R. Moran, *Curr. Opin. Chem. Biol.* **2009**, *13*, 443–450.

Manuscript received: December 01, 2024
Revised manuscript received: July 19, 2025
Accepted manuscript online: July 28, 2025
Version of record online: ■■, ■■